nature nanotechnology

ARTICLES

PUBLISHED ONLINE: 25 MAY 2015 | DOI: 10.1038/NNANO.2015.105

Prescribed nanoparticle cluster architectures and low-dimensional arrays built using octahedral DNA origami frames

Ye Tian[1‡], Tong Wang[2‡], Wenyan Liu[1], Huolin L. Xin[1], Huilin Li[2,3], Yonggang Ke[4,5,6†], William M. Shih[4,5,6] and Oleg Gang[1*]

Three-dimensional mesoscale clusters that are formed from nanoparticles spatially arranged in pre-determined positions can be thought of as mesoscale analogues of molecules. These nanoparticle architectures could offer tailored properties due to collective effects, but developing a general platform for fabricating such clusters is a significant challenge. Here, we report a strategy for assembling three-dimensional nanoparticle clusters that uses a molecular frame designed with encoded vertices for particle placement. The frame is a DNA origami octahedron and can be used to fabricate clusters with various symmetries and particle compositions. Cryo-electron microscopy is used to uncover the structure of the DNA frame and to reveal that the nanoparticles are spatially coordinated in the prescribed manner. We show that the DNA frame and one set of nanoparticles can be used to create nanoclusters with different chiroptical activities. We also show that the octahedra can serve as programmable interparticle linkers, allowing one- and two-dimensional arrays to be assembled with designed particle arrangements.

The assembly of well-defined particle clusters by design has long been seen to be one of the key challenges in rational material fabrication due to their direct analogy with molecules. The designed clusters are not constrained by the orientations of interatomic bonds as in molecules found in the natural world, so a broad diversity of structures can potentially be generated. Clusters with tailored structures and functions could be used as the designer's blocks to create higher-level organizations. Such clusters were recently proposed to address the challenge of inverse engineering in self-assembled systems[1,2]. From a functional perspective, meso-clusters designed from nanoparticles are attractive because of the opportunity to access their collective and synergetic properties[3–6] and to manipulate their optical response[3,7–9].

Recently, much progress has been made on the micrometre scale regarding understanding and fabricating clusters from so-called patchy particles[10], where the placement of patches determines directional interparticle interactions[11,12]. For nanoscale particles, the challenges involved in placing patterns in specified locations with high fidelity are significant, so alternative strategies have been considered. A number of studies have explored DNA-assembled heteroclusters[13], discrete and polymer-like[14] assemblies using nanoparticles with monovalent and multivalent binding properties[4,13–16], stepwise assembly from molecularly encoded surfaces[17] and via templating of molecular motifs[18–20]. Nevertheless, methods for the robust and massive assembly of complex yet designed cluster architectures in which nanoparticles of different types can be spatially arranged in predetermined three-dimensional (3D) arrangements remain challenging. An ultimate goal is the development of a universal assembly platform that can be applied to a wide range of nanoparticle materials and their surface functionalities.

In this Article we propose and demonstrate the experimental realization of a nanoparticle cluster assembly platform using a rigid 3D nanoscale molecular frame. We show, in a specific implementation using an octahedral DNA frame, that nanoparticles can be arranged in three dimensions in prescribed locations determined by the frame vertices encoded by the specific DNA sequences (Fig. 1). We present several representative examples of particle organizations: (1) an octahedral cluster that fully replicates the frame geometry (Fig. 1b); (2) a square-like cluster in which the subset symmetry of the original frame is used (Fig. 1c); and (3) an octahedral heterocluster in which three types of particle are coordinated in particular positions (Fig. 1d). We stress that the demonstrated approach is conceptually different from assembly methods based on patchy and patterned particles, because no complex particle fabrication is required. As we show below, the proposed methodology, 'cluster assembly by frame', streamlines the fabrication of designed 3D meso-architectures and fully supports the integration of different types of nanoparticle containing specific DNAs in their shells[21,22]. We choose to use DNA as a frame for the implementation of the concept due to its highly customizable structure[23] and the ease of programmability of interactions between the frame and particles. Over the past decade, DNA has been a key component in compelling methods for the creation of nanoparticle arrays, either in two dimensions using DNA tile motifs[24,25] and implementing basic design rules[23] or in three dimensions using DNA-encoded particle-shell interactions[26,27], as well as discrete assemblies and linear arrays[4,8,18]. DNA origami technology allows for the designed fabrication of discrete two-dimensional (2D)[28] and 3D[29] DNA shapes, and the reactive groups can be precisely located[30]. Here, we use a 3D origami construct, shaped as an octahedron with DNA-encoded vertices, as a frame for the assembly of

[1]Center for Functional Nanomaterials, Brookhaven National Laboratory, Upton, New York 11973, USA. [2]Biosciences Department, Brookhaven National Laboratory, Upton, New York 11973, USA. [3]Department of Biochemistry and Cell Biology, Stony Brook University, Stony Brook, New York 11794-5213, USA. [4]Department of Biological Chemistry and Molecular Pharmacology, Harvard Medical School, Boston, Massachusetts 02115, USA. [5]Department of Cancer Biology, Dana-Farber Cancer Institute, Boston, Massachusetts 02115, USA. [6]Wyss Institute for Biologically Inspired Engineering, Harvard University, Boston, Massachusetts 02115, USA; †Present address: Department of Biomedical Engineering, Georgia Institute of Technology and Emory University, Atlanta, Georgia 30322, USA. ‡These authors contributed equally to this work. *e-mail: ogang@bnl.gov

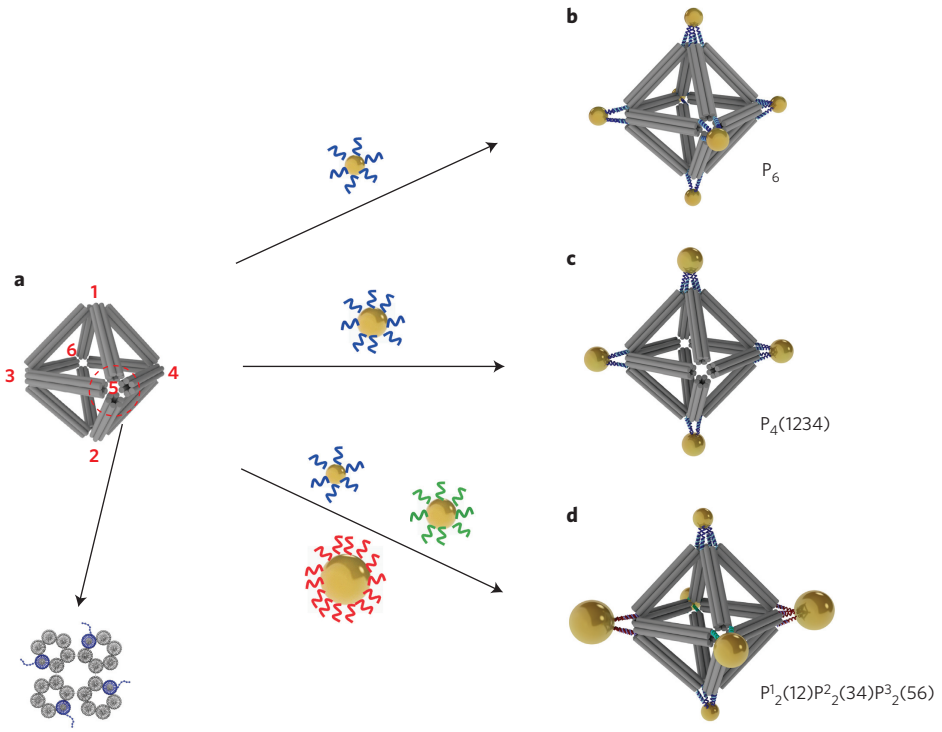

Figure 1 | Scheme of three designed clusters assembled from DNA-functionalized gold nanoparticles on correspondingly encoded vertices of octahedral DNA frames. a, The designed octahedral origami structure. Red numbers indicate the six corners or vertices of the octahedron. One vertex is zoomed (bottom) to show the end-on view of the designed structure composed of four six-helix bundles (6HB). Each 6HB contains one ssDNA sticky end (dotted blue lines) that provides encoding. **b**, An octahedron with all sticky ends encoded to coordinate 7 nm nanoparticles into the symmetric six-nanoparticle cluster P_6. **c**, The $P_4(1234)$ cluster structure may form if the ssDNA at vertices 1-2-3-4 of the octahedral frame is programmed with a sequence complementary to the ssDNA on the 10 nm gold nanoparticles. **d**, The $P^1{}_2(12)P^2{}_2(34)P^3{}_2(56)$ cluster structure may assemble if the ssDNA at vertices 1-2, 3-4 and 5-6 are programmed to complement the ssDNA on the 7 nm, 15 nm and 10 nm nanoparticles, respectively.

designed clusters from nanoparticles. Moreover, we show that their optical response, a chiroptical activity[4,7,8], can be fully controlled based on the prescribed placement of nanoparticles of different sizes on the same central-symmetrical frame. By exploiting the octahedron frame as a programmable linker between nanoparticles, we demonstrate, using *ex situ* transmission electron microscopy (TEM) and *in situ* X-ray scattering methods, that low-dimensional, linear one-dimensional (1D) and square 2D nanoparticle arrays can be successfully created in a designed manner.

Revealing the 3D structure of mesoscale clusters is a significant challenge, in particular due to the need to probe clusters both on ensemble and individual cluster levels at different scales. Such probing of the frame internal structure, the 3D positioning of nanoparticles and a cluster population analysis are important for the realization of high-fidelity assembly and understanding the effects of frame/nanoparticle interactions. Traditional TEM only provides clear images of metal nanoparticles[31], not of the DNA constructs. Negative staining electron microscopy (EM) offers a way of observing both metal particles and the DNA template[8,18,30], but can flatten and thus distort the relatively large 3D structure. In contrast, cryo-electron microscopy (cryo-EM) preserves samples in their near-native states and provides close to nanometre resolution of structures using a single-particle 3D reconstruction technique[24,32–34] and tomography[35–37]. We show here that cryo-EM can be successfully applied to probe the 3D structure of DNA–nanoparticle clusters.

Structure of octahedral frame and prescribed nanoclusters

First, we designed the frame, an octahedral DNA origami structure (Fig. 1a)[38] with each edge containing a six-helix bundle (6HB)[39–41]. Vertex positions (labelled 1 to 6) can be encoded with distinctive single-stranded DNA (ssDNA) 'sticky ends', which can bind nanoparticles coated with complementary DNA. We designed three routes to assemble different numbers and sizes of gold nanoparticles (Fig. 1b–d). When six vertices have the same sticky end, a six-particle cluster is formed after mixing with the corresponding DNA-encoded nanoparticles. The resulting nanoparticle cluster, denoted 'P_6' (Fig. 1b), has symmetry O_h. When only four in-plane vertices are encoded and two others are silent, a four-particle cluster (Fig. 1c) can be formed, denoted '$P_4(1234)$' to indicate the number of particles and their vertex locations. A heterogeneous cluster can be created by introducing different DNA at chosen vertices. Here, we have used three distinctive sets of sticky ends, with two of the same kind located at opposite vertices (Fig. 1d). Such a design allows three types of nanoparticle to be bound. We used 7 nm (P^1), 10 nm (P^2) and 15 nm (P^3) gold nanoparticles (Supplementary Section C) with respectively complementary shells for prescribing this heterocluster, labelled as '$P^1{}_2(12)P^2{}_2(34)P^3{}_2(56)$'. The high-fidelity octahedral formation (with a TEM observed yield of ~99%) is clearly visible in the raw cryo-EM micrograph in Fig. 2a. The DNA octahedra are randomly oriented in the vitreous ice, have the expected dimensions, and appear monodisperse in shape and size. These 2D images permitted computational reconstruction of the 3D structure of the octahedron origami (Supplementary Section H), as we discuss in the following. The 2D class averages of raw particle images are nearly identical to the corresponding reprojections of the reconstructed 3D density model (Fig. 2b). This demonstrates the quality of the particle images and the reliability of the 3D reconstruction of the DNA octahedron.

The 3D density map was surface-rendered and is shown in the typical four-fold, three-fold and two-fold axis views in Fig. 2c. The octahedral edge in the 3D map is ~29 nm long, in agreement with the designed length of 28.6 nm. Each edge of the reconstructed

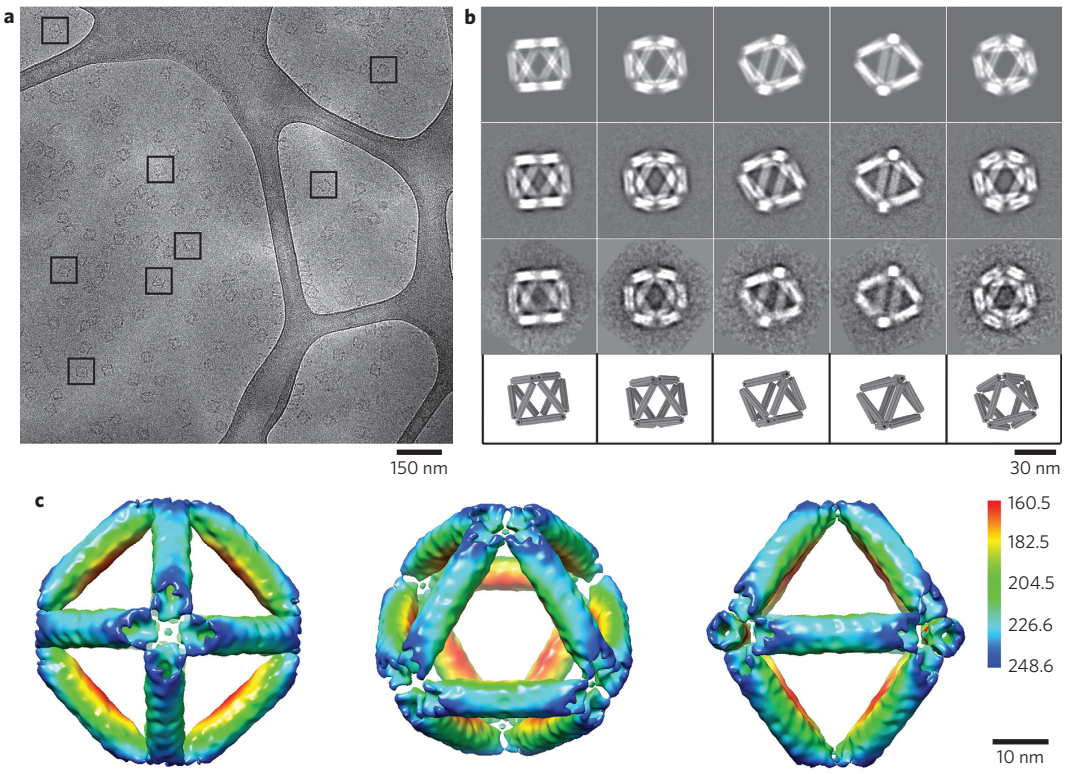

Figure 2 | Structure of the self-assembled DNA origami octahedron, obtained by cryo-EM and 3D reconstruction. a, A cryo-EM micrograph with representative views of the DNA octahedron enclosed by black squares. Only cluster structures that were embedded in the vitreous ice and suspended over the irregular holes in the carbon film substrate were selected for further analysis. **b**, Comparison of 2D re-projections of the reconstructed 3D density map (top row) with reference-based class averages (second row), reference-free class averages (third row) and the corresponding views of the 3D design model (bottom row). **c**, Surface-rendered 3D density maps of the DNA octahedron, viewed from the four-fold (left), three-fold (middle) and two-fold (right) symmetry axes. The density surface is coloured radially from interior red to outer blue. The colour key is shown on the right. Values in the colour key indicate the distance in ångströms from the octahedral centre.

DNA octahedron is a hollow structure with a ~2 nm channel in the middle. Again, this feature is consistent with our six-helix bundle design for the edge (Fig. 1 and Supplementary Fig. 3). We therefore chose the six-helix bundle (6HB) design to construct octahedron edges. The hollow structure of 6HB and the octahedral vertices formed provide housing functionalized moieties, with potential applications in nanotechnology and biomedicine[30]. Our success in visualizing the structure of the large, symmetric and non-space-filling 3D origami constructs by cryo-EM is notable, because, to date, this method has only been applied to space-filling DNA origami[34] or the flexible origami box[32] or to nanoscale non-origami polyhedra[24,32,33].

We next assembled a simple P_6 cluster on the octahedron frame using 30-base ssDNA-functionalized 7 nm gold nanoparticles. Figure 3a presents a representative raw image of the purified complexes. These clusters are highly homogeneous, with over 90% of the 460 clusters counted containing the correct number (six) of nanoparticles in the prescribed vertex positions in each octahedron (Fig. 3a, inset).

It is clear that the six nanoparticles of the individual clusters in the raw cryo-EM images are arranged in a manner that is consistent with the octahedral symmetry (Fig. 3b). Notably, the DNA is barely visible, with much weaker contrast than the gold nanoparticles. This is because the gold nanoparticles are significantly more electron dense than the DNA. We therefore calculated two independent 3D reconstructions from the same cryo-EM data set. In the first, the high nanoparticle densities were computationally removed from the raw images, keeping the DNA density intact (Supplementary Fig. 5b). In the second, the lower-intensity DNA density and the background noise were removed, leaving only the higher-intensity nanoparticles (Supplementary Fig. 5c). We normalized and then aligned the two reconstructions by their symmetry axes and merged them into a synthetic structure (Fig. 3c). In this compound map, the diameters of nanoparticles are ~7 nm, consistent with the particle size estimated from the raw images. Six nanoparticles are precisely positioned at the six vertices of the reconstructed DNA octahedron frame, with a nearest centre-to-centre interparticle distance of ~42 nm.

Control over the assembly of predefined cluster $P_4(1234)$, with its square-like particle arrangement, was further demonstrated by choosing four co-planar corners of the octahedron to have the specific sticky end oligonucleotides (Fig. 1c). Nanoparticles (10 nm) with complementary ssDNA shells were assembled into this P_4 cluster. The population histogram in Fig. 3d demonstrates that ~80% of the clusters contain the correct number (four) of nanoparticles (of a total of 554). Figure 3e compares cryo-EM images of six representative origami nanoparticle clusters with the corresponding views from the 3D model. To illustrate the arrangement of the four nanoparticles on the DNA octahedra, we computed a composite map (Fig. 3f) by aligning and merging the gold nanoparticles reconstruction with the DNA octahedron reconstruction, shown in Fig. 2c. The nanoparticle size in the reconstruction is ~10 nm, consistent with the estimate from the raw images, and the nearest centre-to-centre interparticle distance is ~40 nm. Thus, four nanoparticles are precisely positioned at the predefined octahedron vertices forming the prescribed P_4 cluster.

We next demonstrate that the outlined assembly approach allows for the realization of heteroclusters containing several types of particles in predefined positions. For example, the cluster was designed to coordinate three particle types, $P^1{}_2(12)P^2{}_2(34)P^3{}_2(56)$, as shown in Fig. 1d.

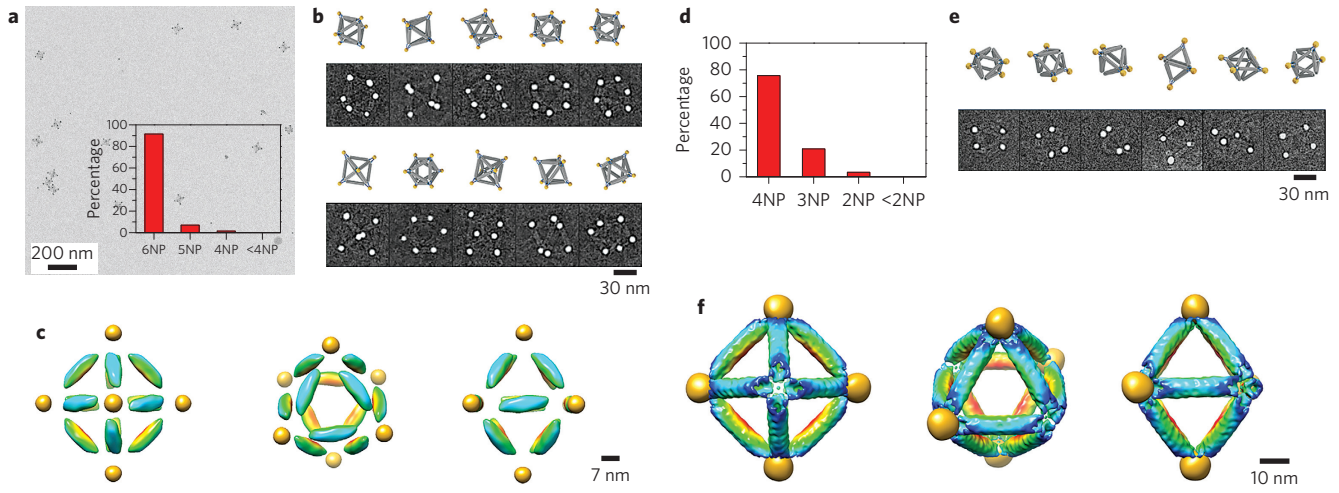

Figure 3 | Structure of six-fold P_6 and four-fold $P_4(1234)$ nanoparticle clusters, as revealed by cryo-EM and 3D reconstruction. a, Representative EM image of the P_6 cluster structure. Inset: histogram of assembled clusters with observed nanoparticle numbers. **b**, Comparison of ten selected raw cryo-EM images of the fully assembled P_6 octahedron–nanoparticle clusters (second and fourth rows) with corresponding views from the 3D design model (first and third rows). **c**, Composite 3D EM structure of the P_6 cluster derived by computationally combining the structures shown in Supplementary Fig. 5b,c. The left, middle and right panels show four-fold, three-fold and two-fold views of the structure. **d**, Cluster population histogram for $P_4(1234)$. **e**, Comparison of six selected raw cryo-EM images of the assembled $P_4(1234)$ cluster (bottom row) with corresponding views from the design model (top row). **f**, Composite density map of the $P_4(1234)$ cluster derived by combining 3D reconstruction of the DNA octahedron (Fig. 2c) with 3D reconstruction of the four 10 nm nanoparticles organized by the octahedral DNA frame. The rendering threshold of the latter is set to show the nanoparticle densities. Left, middle and right panels: views along the four-fold, three-fold and two-fold symmetry axes of the octahedron. Density surfaces of the DNA octahedron in **c** and **f** are coloured in the same way as that in Fig. 2c.

The six corners of the octahedron were grouped into three diagonal sets. By providing the corresponding DNA encoding, we assign vertices 1 and 2, 3 and 4, and 5 and 6 to bind to 7 nm, 10 nm and 15 nm nanoparticles, respectively. The representative TEM image of the assembled cluster shows that the majority of these clusters have the correct structure (Supplementary Fig. 8). The population histogram in Fig. 4a reveals that ~70% of the clusters (from a total of 467 clusters) coordinate six nanoparticles with about equal fractions of each particle type. For partially assembled clusters (five nanoparticles or less) the missing nanoparticles are of three different particle types, in nearly even proportions. Note that the DNA is nearly invisible because of the high dynamical range of electron densities.

To unravel the 3D coordinates of the assembled $P^1{}_2P^2{}_2P^3{}_2$ cluster, we applied a tomographic method for this system, which permits 3D probing of individual clusters. The TEM image in the inset to Fig. 4a presents an untilted view of the cluster, which corresponds to the reconstructed particle positions in Fig. 4b, while Fig. 4c presents a few selected tilted images of the reconstruction at tilt angles of −20°, −10°, 20°, 40° and 60°. The projections of the reconstructed clusters agree well with the raw EM images. The average surface-to-surface distances (d_7, d_{10} and d_{15}) between nanoparticles of the same size (7 nm, 10 nm and 15 nm, respectively) were obtained from twelve reconstructed clusters (Fig. 4d). A small but progressive decrease in interparticle distance by ~4 nm is observed when the nanoparticle diameter decreases from 15 nm to 7 nm. This change may result from the different curvature of the particles, arising from the dependence of DNA length in a shell on particle size[42]. Also, due to the larger attachment area of the DNA of a vertex with bigger particles, a strain might be imposed on the octahedron, resulting in its distortion. Average basal (α) and vertex (β, for a 15 nm nanoparticle) angles, as noted in Fig. 4b, exhibit the well-defined positions of all nanoparticles attached to an octahedral frame (Fig. 4e). The ideal basal angle is ~90°, which matches our experimental data, while the vertex angle (54.5° ± 10.0°) is close to the expected value of ~56°. We therefore conclude that even the attachment of larger particles (15 nm Au core) introduces practically no distortion on the frame, further supporting the potential use of this approach for the assembly of various designer heteroclusters.

Chiroptical activity of heteroclusters

The ability to assemble nanoparticle clusters in a designed manner opens new opportunities for creating materials with regulated functions. For example, chiroptical activity might be induced in plasmonically coupled spherical nanoparticles placed on a chiral[8] or tetrahedral scaffold[4]. However, as we show here, even a centre-symmetric frame such as an octahedron allows a chiroptical response to be produced if particles of different sizes are placed appropriately. In this case, the chirality is determined by the position of specifically encoded vertices that, in turn, prescribe the placement of different particles. More specifically, depending on the arrangement of nanoparticles of three sizes on the vertices of the octahedron, either in a symmetric fashion (similar to $P^1{}_2P^2{}_2P^3{}_2$; Fig. 4b) or non-symmetrically, non-chiral or chiral architectures can be formed (Fig. 5a,b). Thus, from the same set of particles and the same, but differently encoded, octahedron frame, different chiroptical signatures can be generated.

To realize this idea experimentally, we substituted the 7 nm P_1 particle in $P^1{}_2P^2{}_2P^3{}_2$ with 20 nm gold nanoparticle P_4 in order to increase the cluster plasmonic response. The new cluster, $P^2{}_2(34)P^3{}_2(56)P^4{}_2(12)$, denoted $P^2{}_2P^3{}_2P^4{}_2$ (Fig. 5a), has the same-sized particles placed symmetrically (see also the cluster top view in Fig. 5a). A representative TEM image of the $P^2{}_2P^3{}_2P^4{}_2$ cluster with the correspondingly oriented model are shown in the top right inset of Fig. 5c. No circular dichroism (CD) signal was detected in the plasmonic region of the spectrum (Fig. 5c, red line) for this cluster. However, when the three pairs of nanoparticles were positioned in an asymmetric arrangement (Fig. 5b), the resulting octahedral cluster had left-handed chirality[43], as verified by the anticlockwise rotation of the 1-3-5 positions of distinguished particles to match the 4-6-2 positions of their twins. Indeed, cluster $P^2{}_2(36)P^3{}_2(25)P^4{}_2(14)$, denoted $P^2{}_{c2}P^3{}_{c2}P^4{}_{c2}$, contains three

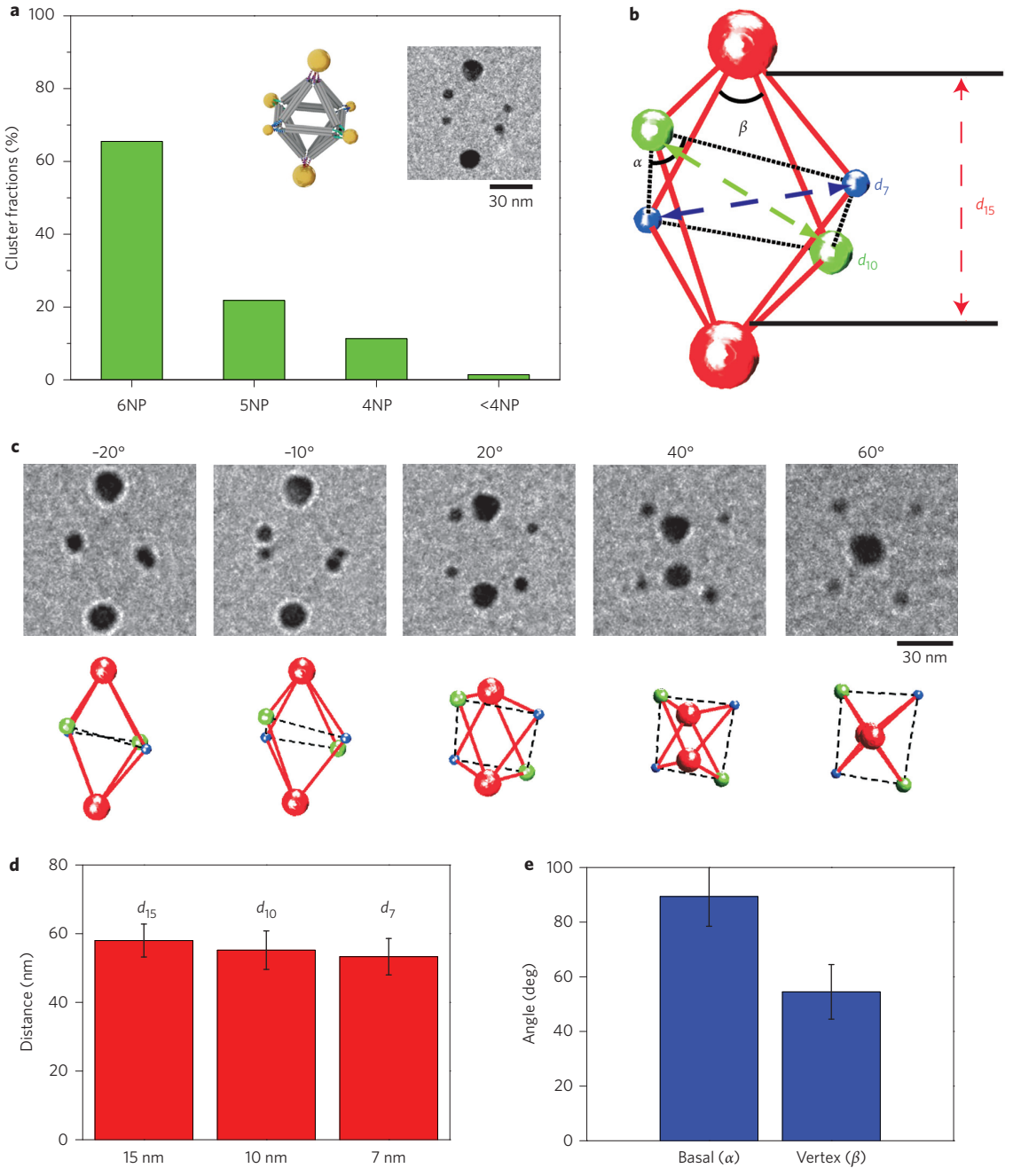

Figure 4 | Characterization of heterocluster population and structure of individual heteroclusters, $P^1_2(12)P^2_2(34)P^3_2(56)$. a, Statistical analysis of the nanoparticle cluster population. Insets: design model and representative cryo-EM image of the assembled cluster (untilted view). **b**, Reconstructed 3D structure of the nanoparticle cluster shown in the inset of **a**. The surface-to-surface distance between the diagonally paired 7 nm, 10 nm and 15 nm nanoparticles are denoted d_7, d_{10} and d_{15}, respectively. α is the basal angle centred around the 10 nm nanoparticles and β the vertex angle around the 15 nm nanoparticles. **c**, Comparison of images obtained by tilting the cluster shown in **a** at different angles (top row) with corresponding views of the reconstructed 3D structure. **d**, Averaged distances between the diagonally paired 7, 10 and 15 nm nanoparticles measured from 12 independently reconstructed $P^1_2P^2_2P^3_2$ clusters: $d_{15} = 58.0 \pm 4.8$ nm, $d_{10} = 55.1 \pm 5.6$ nm and $d_7 = 53.3 \pm 5.3$ nm. **e**, Averaged values of the basal ($\alpha = 89.4° \pm 10.9°$) and vertex ($\beta = 54.5° \pm 10.0°$) angles.

nanoparticle pairs with the same types of nanoparticles placed at the edge ends. A representative TEM image and the corresponding model are shown in the bottom left inset of Fig. 5c. For this $P^2_{c2}P^3_{c2}P^4_{c2}$ cluster, a negative CD signal was observed (Fig. 5c, black line), with its centre at the plasmonic peak of the gold cluster (for absorption curves see Supplementary Fig. 12), corresponding to the cluster's left-handed structural chirality. We note that only a very small difference (<1 nm) was observed between the plasmonic peak positions for both cases, whereas dramatically different chiroptical responses are exhibited for the symmetric and asymmetric clusters. Interestingly, even the weak plasmonic coupling between nanoparticles (Supplementary Fig. 12) in our system (due to the relatively large separations; ~36 nm surface-to-surface distances) can still be translated into an observable CD response. We have therefore demonstrated that the same set of nanoparticles and the same centre-symmetric frame can be used

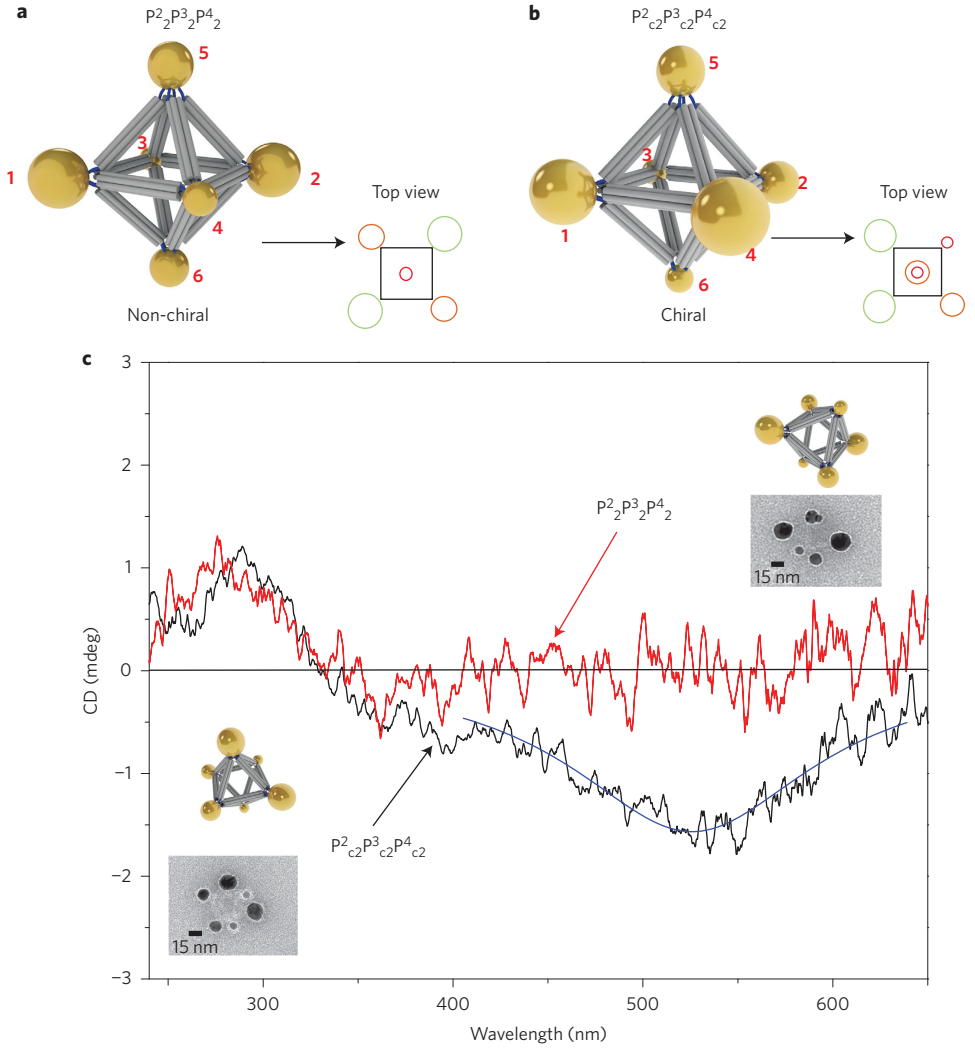

Figure 5 | CD spectra for non-chiral and chiral nanoparticle clusters assembled on an octahedron frame. a, Model of non-chiral cluster $P^2{}_2P^3{}_2P^4{}_2$ and a top view. **b**, Model of chiral cluster $P^2{}_{c2}P^3{}_{c2}P^4{}_{c2}$ with a top view. **c**, Red line: CD spectrum for cluster $P^2{}_2P^3{}_2P^4{}_2$. A representative TEM image and the model with the same orientation are shown (top right). Black line: CD spectrum for cluster $P^2{}_{c2}P^3{}_{c2}P^4{}_{c2}$. Blue line: Lorentzian fit. A representative TEM image and model with the same orientation are shown (bottom left). The CD peaks at ~270 nm for both types of cluster are DNA signatures.

to produce clusters with optically different CD responses by means of a simple, but precise, spatial placement of the nanoparticles into the 3D cluster.

Designed 1D and 2D nanoparticle arrays

We further explored the use of the specifically encoded octahedron frame as a linking element between nanoparticles for building low-dimensional, 1D and 2D, nanoparticle arrays. In this case the linking symmetry and the resulting structure of the array were determined by the choice of octahedron vertices utilized for interparticle connections. Unlike assembly approaches using particle positioning on DNA scaffolds, in the present strategy nanoparticles and DNA are integrated in the unified structure, and the topology of the interparticle connections is fully prescribed by the encoding of the octahedra vertices. We prescribe these 1D and 2D arrays by encoding the octahedron to carry two-fold (Fig. 6a) and four-fold (Fig. 6d) symmetries, respectively. More specifically, the frame with two-fold symmetry contains two vertices with encoding for particle recognition at two ends of the major octahedron diagonal. Consequently, this design should result in linear arrangements of nanoparticles linked by the two-fold linking frame. Expanding this approach, we can direct the assembly of a 2D square array (D4 symmetry) by encoding the four octahedron vertices, lying in the same plane, for nanoparticle binding. Details for obtaining a low-dimensional array are described in the Methods. The samples were then loaded into glass capillaries and probed by small angle X-ray scattering (SAXS), as described previously[21,26].

A plot of the structure factor for the nanoparticle assembly induced by the two-fold encoded octahedron (Fig. 6c) exhibits five peaks, with peak positions located at $q/q_1 \approx 1, 1.8, 2.7, 3.5$ and 4.3 (q_1 is the position of the first peak). Such a structure factor profile can be reasonably well described (Fig. 6c, blue curve) by a dumbbell model[44,45] with the functional form $S(q) \approx \sin(dq)/dq$, where d is the distance between nanoparticle centres, indicating the scattering signature of the nanoparticle pairs. The flexibility of the 1D array at the points of octahedron attachment to nanoparticles and the large angle over which the attachment can occur contribute to the non-collinearity of the 1D array. The fit yields $d = 67.4$ nm, which is close to the expected value based on the design parameters. We further confirmed (Fig. 6b) the structure of this array by TEM imaging, which shows the morphology and inter-nanoparticle distance ($d \approx 57$–63 nm) to be in agreement with the *in situ* SAXS results.

The assembly structure induced by the octahedron with four-fold symmetry nanoparticle connections was initially revealed by SAXS.

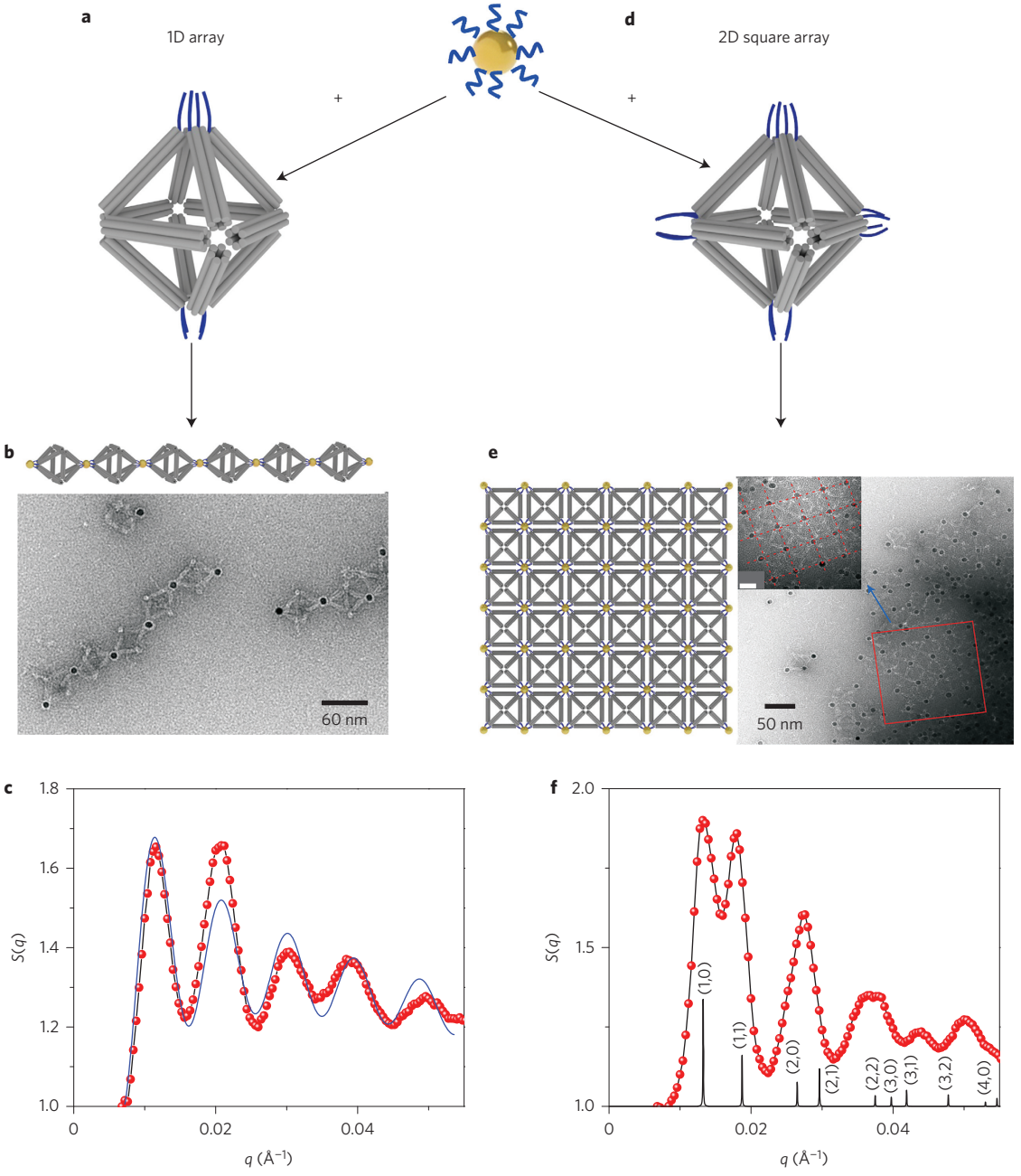

Figure 6 | Correspondingly encoded octahedra used as programble linkers for assembly into linear and 2D square arrays, respectively. a, Model of octahedral DNA origami with two-fold symmetry nanoparticle binding for assembly of a 1D array. **b**, Model of the 1D array (top) and representative negative stained TEM image of the formed 1D array (bottom). **c**, Extracted structure factor $S(q)$ for the 1D array from the *in situ* SAXS pattern (red symbols, measurements; blue line, fitting as described in the text). **d**, Model of the octahedral DNA origami with four-fold symmetry nanoparticle binding for the assembly of a 2D square array. **e**, Model of the 2D square array and representative negative stained TEM image of the formed 2D nanoparticle–octahedra array (inset: zoomed picture of selected area; scale bar, 25 nm). **f**, Extracted structure factor $S(q)$ for the 2D nanoparticle array (red symbols) and the simulated 2D scattering pattern (black lines with corresponding diffraction peak indexes).

The observed $S(q)$ peaks signify a 2D nanoparticle square array (Fig. 6f) with an interparticle distance of 47.5 nm, which is in agreement with the value of 46.4 nm obtained from the model. The deviation of higher-order peaks from the calculated values towards larger q can be attributed to the flexibility of the 2D nanoparticle–octahedron sheet in solution. Such a structure agrees with the array design (Fig. 6e, left model). Indeed, in the formed 2D square arrays, the four in-plane vertices (Fig. 6d) are bound to four gold nanoparticles, and each nanoparticle binds four octahedra (the vertices below and above the plane are silent). The size of 2D crystallites is 0.2 μm, as estimated from the scattering peak width, and their melting temperature is ~39 °C, as detected by dynamic light scattering measurements (Supplementary Fig. 14). The *ex situ* visualization with TEM (Fig. 6e, right) concurs with the SAXS results and closely resembles the model arrangement: a 2D square array of nanoparticles that are linked by a four-fold binding octahedron.

Conclusions

The presented studies demonstrate that 3D nanoparticle clusters can be created effectively using a strategy based on a rigid 3D DNA frame with encoded sites for nanoparticle positioning. Our example of such an approach based on an octahedron allows for particles to be

arranged in three dimensions with nearly nanometre precision in the designed non-periodic structure, as confirmed by a detailed visualization using cryo-EM methods. Based on such precise cluster assembly, nano-architectures with different chiroptical activities were created using the same set of nanoparticles but different frame encodings. Moreover, we have demonstrated that designed arrangement of nanoparticles in 1D and 2D arrays could be achieved by prescribing specific vertices of the octahedron as nanoparticle connecting sites. The structural integrity of the DNA frame ensures proper nanoparticle coordination, while the DNA origami methodology provides predictable frame fabrication. Our work opens up numerous exciting opportunities for high-yield precise assembly of tailored 3D mesoscale building blocks in which multiple nanoparticles of different structures and functions can be integrated.

Methods

Methods and any associated references are available in the online version of the paper.

Received 13 June 2014; accepted 20 April 2015; published online 25 May 2015

References

1. Halverson, J. D. & Tkachenko, A. V. DNA-programmed mesoscopic architecture. *Phys. Rev. E* **87,** 062310 (2013).
2. Zeravcic, Z. & Brenner, M. P. Self-replicating colloidal clusters. *Proc. Natl Acad. Sci. USA* **111,** 1748–1753 (2013).
3. Maye, M. M., Gang, O. & Cotlet, M. Photoluminescence enhancement in CdSe/ZnS-DNA linked-Au nanoparticle heterodimers probed by single molecule spectroscopy. *Chem. Commun.* **46,** 6111–6113 (2010).
4. Yan, W. *et al.* Self-assembly of chiral nanoparticle pyramids with strong *R/S* optical activity. *J. Am. Chem. Soc.* **134,** 15114–15121 (2012).
5. Fan, J. A. *et al.* Plasmonic mode engineering with templated self-assembled nanoclusters. *Nano Lett.* **12,** 5318–5324 (2012).
6. Hiroi, K., Komatsu, K. & Sato, T. Superspin glass originating from dipolar interaction with controlled interparticle distance among gamma-Fe_2O_3 nanoparticles with silica shells. *Phys. Rev. B* **83,** 224423 (2011).
7. Govorov, A. O., Fan, Z., Hernandez, P., Slocik, J. M. & Naik, R. R. Theory of circular dichroism of nanomaterials comprising chiral molecules and nanocrystals: plasmon enhancement, dipole interactions, and dielectric effects. *Nano Lett.* **10,** 1374–1382 (2010).
8. Kuzyk, A. *et al.* DNA-based self-assembly of chiral plasmonic nanostructures with tailored optical response. *Nature* **483,** 311–314 (2012).
9. Barrow, S. J., Wei, X., Baldauf, J. S., Funston, A. M. & Mulvaney, P. The surface plasmon modes of self-assembled gold nanocrystals. *Nature Commun.* **3,** 1–9 (2012).
10. Ruzicka, B. *et al.* Observation of empty liquids and equilibrium gels in a colloidal clay. *Nature Mater.* **10,** 56–60 (2011).
11. Wang, Y. *et al.* Colloids with valence and specific directional bonding. *Nature* **491,** 51–56 (2012).
12. Chen, Q. *et al.* Supracolloidal reaction kinetics of janus spheres. *Science* **331,** 199–202 (2011).
13. Mastroianni, A. J., Claridge, S. A. & Alivisatos, A. P. Pyramidal and chiral groupings of gold nanocrystals assembled using DNA scaffolds. *J. Am. Chem. Soc.* **131,** 8455–8459 (2009).
14. Klinkova, A., Thérien-Aubin, H., Choueiri, R. M., Rubinstein, M. & Kumacheva, E. Colloidal analogs of molecular chain stoppers. *Proc. Natl Acad. Sci. USA* **110,** 18775–18779 (2013).
15. Kim, J-W., Kim, J-H. & Deaton, R. DNA-linked nanoparticle building blocks for programmable matter. *Angew. Chem. Int. Ed.* **50,** 9185–9190 (2011).
16. Alivisatos, A. P. *et al.* Organization of 'nanocrystal molecules' using DNA. *Nature* **382,** 609–611 (1996).
17. Maye, M. M., Nykypanchuk, D., Cuisinier, M., van der Lelie, D. & Gang, O. Stepwise surface encoding for high-throughput assembly of nanoclusters. *Nature Mater.* **8,** 388–391 (2009).
18. Pal, S., Deng, Z., Ding, B., Yan, H. & Liu, Y. DNA-origami-directed self-assembly of discrete silver-nanoparticle architectures. *Angew. Chem. Int. Ed.* **49,** 2700–2704 (2010).
19. Lee, J., Hernandez, P., Govorov, A. O. & Kotov, N. A. Exciton–plasmon interactions in molecular spring assemblies of nanowires and wavelength-based protein detection. *Nature Mater.* **6,** 291–295 (2007).
20. Sun, D. *et al.* Heterogeneous nanoclusters assembled by PNA-templated double-stranded DNA. *Nanoscale* **4,** 6722–6725 (2012).
21. Zhang, Y., Lu, F., Yager, K. G., van der Lelie, D. & Gang, O. A general strategy for the DNA-mediated self-assembly of functional nanoparticles into heterogeneous systems. *Nature Nanotech.* **8,** 865–872 (2013).
22. Zhang, C. *et al.* A general approach to DNA-programmable atom equivalents. *Nature Mater.* **12,** 741–746 (2013).
23. Seeman, N. C. DNA in a material world. *Nature* **421,** 427–431 (2003).
24. Shih, W. M., Quispe, J. D. & Joyce, G. F. A 1.7-kilobase single-stranded DNA that folds into a nanoscale octahedron. *Nature* **427,** 618–621 (2004).
25. Zheng, J. *et al.* From molecular to macroscopic via the rational design of a self-assembled 3D DNA crystal. *Nature* **461,** 74–77 (2009).
26. Nykypanchuk, D., Maye, M. M., van der Lelie, D. & Gang, O. DNA-guided crystallization of colloidal nanoparticles. *Nature* **451,** 549–552 (2008).
27. Park, S. Y. *et al.* DNA-programmable nanoparticle crystallization. *Nature* **451,** 553–556 (2008).
28. Rothemund, P. W. K. Folding DNA to create nanoscale shapes and patterns. *Nature* **440,** 297–302 (2006).
29. Dietz, H., Douglas, S. M. & Shih, W. M. Folding DNA into twisted and curved nanoscale shapes. *Science* **325,** 725–730 (2009).
30. Zhang, C. *et al.* DNA nanocages swallow gold nanoparticles (AuNPs) to form AuNP@DNA cage core–shell structures. *ACS Nano* **8,** 1130–1135 (2014).
31. Sharma, J. *et al.* Control of self-assembly of DNA tubules through integration of gold nanoparticles. *Science* **323,** 112–116 (2009).
32. Andersen, E. S. *et al.* Self-assembly of a nanoscale DNA box with a controllable lid. *Nature* **459,** 73–76 (2009).
33. He, Y. *et al.* Hierarchical self-assembly of DNA into symmetric supramolecular polyhedra. *Nature* **452,** 198–201 (2008).
34. Bai, X., Martin, T. G., Scheres, S. H. W. & Dietz, H. Cryo-EM structure of a 3D DNA-origami object. *Proc. Natl Acad. Sci. USA* **149,** 20012–20017 (2012).
35. Midgley, P. A. & Dunin-Borkowski, R. E. Electron tomography and holography in materials science. *Nature Mater.* **8,** 271–280 (2009).
36. Kourkoutis, L. F., Plitzko, J. M. & Baumeister, W. Electron microscopy of biological materials at the nanometer scale. *Annu. Rev. Mater. Res.* **42,** 33–58 (2012).
37. De-Rosier, D. & Klug, A. Reconstruction of three dimensional structures from electron micrographs. *Nature* **217,** 130–134 (1968).
38. Douglas, S. M. *et al.* Rapid prototyping of 3D DNA-origami shapes with caDNAno. *Nucleic Acids Res.* **37,** 5001–5006 (2009).
39. Mathieu, F. *et al.* Six-helix bundles designed from DNA. *Nano Lett.* **5,** 661–665 (2005).
40. Douglas, S. M. *et al.* Self-assembly of DNA into nanoscale three-dimensional shapes. *Nature* **459,** 414–418 (2009).
41. Douglas, S. M., Chou, J. J. & Shih, W. M. DNA-nanotube-induced alignment of membrane proteins for NMR structure determination. *Proc. Natl Acad. Sci. USA* **104,** 6644–6648 (2006).
42. Hill, H. D., Millstone, J. E., Banholzer, M. J. & Mirkin, C. A. The role radius of curvature plays in thiolated oligonucleotide loading on gold nanoparticles. *ACS Nano* **3,** 418–424 (2009).
43. King, R. B. Nonhanded chirality in octahedral metal complexes. *Chirality* **13,** 465–473 (2001).
44. Chi, C., Vargas-Lara, F., Tkachenko, A. V., Starr, F. W. & Gang, O. Internal structure of nanoparticle dimers linked by DNA. *ACS Nano* **6,** 6793–7802 (2012).
45. Kaya, H. Scattering from cylinders with globular end-caps. *J. Appl. Crystallogr.* **37,** 223–230 (2004).

Acknowledgements

The authors thank J. Li for help with tomography analysis and D. Chen for assistance with schematic drawing. Research carried out at the Centre for Functional Nanomaterials, Brookhaven National Laboratory, was supported by the US Department of Energy, Office of Basic Energy Sciences (contract no. DE-SC0012704). H.L. was supported by a National Institutes of Health R01 grant (AG029979) and W.M.S. was supported by a National Science Foundation Expeditions grant (1317694) and Designing Materials to Revolutionize and Engineer Our Future grant (1435964).

Author contributions

Y.T. and O.G. conceived and designed the experiments. Y.T. performed the experiments. W.M.S. and Y.K. contributed to the octahedral design. Y.T., T.W., W.L. and O.G. analysed the data. T.W. and H.L. contributed to the cryo-EM measurement and reconstruction. H.X. contributed to the tomography analysis. Y.T. and O.G. wrote the paper. O.G. supervised the project. All authors discussed the results and commented on the manuscript.

Additional information

Supplementary information is available in the online version of the paper. Reprints and permissions information is available online at www.nature.com/reprints. Correspondence and requests for materials should be addressed to O.G.

Competing financial interests

The authors declare no competing financial interests.

Methods

Design and folding of DNA octahedral frame. The DNA origami structure was designed using the caDNAno software package (http://cadnano.org/). Each edge of the octahedron is composed of a six-helix bundle (length of ~28.6 nm), one helix of which has a ssDNA extending out of the duplex ends for the attachment of nanoparticles. The octahedral DNA frame was formed by mixing M13mp18 DNA and hundreds of staple strands (Supplementary Section D), slowly annealing from 90 °C to room temperature, then confirmed first by gel electrophoresis (Supplementary Fig. 1).

Model fit of reconstructed octahedron. A standard B-DNA model was built, computationally, to be 84 base pairs in length, then six copies were manually arranged to form a close-packed 6HB DNA model, leaving a hollow channel in the middle (Supplementary Fig. 3). The 6HB model was docked as one entity (rigid body) into one edge of the DNA octahedron EM map, and it was found that the model fitted the density very well (Supplementary Fig. 3). The good agreement led us to conclude that we had succeeded in fabricating the intended DNA origami octahedron. The central cavity of the octahedron was designed such that it could accommodate a spherical particle with a diameter of up to 20 nm.

Preparation of octahedral frame-based nanoclusters. For the assembly of each type of cluster shown in Fig. 1b–d, gold nanoparticles were first mixed with each designed frame in the ratio of 2.5*N*:1 (where *N* indicates number of corners with sticky ends). The mixture was annealed from 50 °C to room temperature overnight, concentrated, and loaded into agarose gel (1%) for separation. The gel band containing assembled clusters was cut out, crushed with a pestle, and filtered through a cellulose-acetate spin column, and the collected sample solution was used for negative stain EM and cryo-EM.

Assembly of low-dimensional arrays. Each design of octahedron was mixed with 10 nm gold nanoparticles in the ratio 1:1. After careful annealing (0.3 °C h^{-1} from 50 °C to 20 °C), red loose precipitates or black aggregates appeared gradually for 1D and 2D cases, respectively.

SAXS profiles. SAXS measurements were performed at the BNL National Synchrotron Light Source (NSLS) X-9 beamline. The samples were injected into glass capillary tubes for X-ray scattering experiments, which were performed under temperature-controlled conditions. Two-dimensional scattering patterns were collected using an area detector. Structure factors $S(q)$, where q is the wavevector, were obtained by the radial integration of 2D patterns and were normalized by a nanoparticle form factor obtained from the scattering of solution-dispersed nanoparticles.